Int J Adv Manuf Technol (2017) 91:3775–3788
DOI 10.1007/s00170-017-0034-6

ORIGINAL ARTICLE

Investigations on feasibility of low-frequency vibration-assisted turning

Naresh Kumar Maroju[1] · **Krishna P. Vamsi**[2] · **Jin Xiaoliang**[1]

Received: 11 September 2016 / Accepted: 9 January 2017 / Published online: 30 January 2017

Abstract Vibration-assisted turning (VAT) is a technique to impose controlled external vibration on original cutting motion of turning process in order to improve part accuracy, surface quality, and tool life. In this study, the mechanics of orthogonal turning with low-frequency (less than 1000 Hz) vibration assistance is investigated. Finite element simulations are conducted to predict and compare the stresses, forces, and temperature between conventional turning (CT) and low-frequency vibration-assisted turning (LVAT). Turning experiments with vibration assistance achieved by electromagnetic actuator are conducted to validate the finite element (FE) model. The effect of vibration assistance on machining performance is quantitatively determined for three typical aerospace materials: Ti6Al4V, AISI 4340, and Al 2024 T351. It is found that LVAT is effective in reducing cutting forces, effective stresses, and cutting temperature. Compressive residual stresses are dominant in LVAT due to the added vibration. Tool wear and surface roughness in LVAT are also experimentally characterized and analyzed.

Keywords Low-frequency turning · Vibration-assisted machining · FEA simulation · Residual stress

✉ Naresh Kumar Maroju
naresh_kumar.maroju@okstate.edu

Krishna P. Vamsi
vamsikrishna@nitw.ac.in

Jin Xiaoliang
xiaoliang.jin@okstate.edu

[1] School of Mechanical and Aerospace Engineering, Oklahoma State University, Stillwater, OK 74075, USA

[2] Department of Mechanical Engineering, National Institute of Technology Warangal, Warangal, Telangana 506004, India

1 Introduction

Continuous efforts have been made to improve the machining performance for aerospace manufacturing, such as optimizing machining parameters, developing innovative machining techniques, and enhancing structure stiffness. One such novel machining method is vibration-assisted machining (VAM), which has shown promising results in improving machining efficiency and part quality [1]. The primary feature of VAM is that the tool-workpiece contact becomes intermittent due to applied vibration assistance, which reduces effective stresses, cutting forces, cutting temperature, tool wear, and surface roughness [2–4]. The intermittent tool-workpiece contact is periodic with repeated penetration and retraction of the cutting tool. Hence, the time spent in actual cutting is less compared to overall machining time and results in stress release in material deformation zone. The machining temperature is relatively low compared to that in conventional machining due to periodic separation between the tool and the workpiece [5]. In addition, the volume of material removed in each vibration cycle is smaller in VAM compared to that in conventional machining (CM). The cutting forces vary due to intermittent tool-workpiece contact, as opposed to constant cutting forces in CM [6]. Overall, the reduction in forces, stresses, and temperature results in better surface finish and improved tool life [3, 7].

Vibration assistance has been applied in both conventional and unconventional machining processes [2]. High-frequency vibration assistance (5 to 40 kHz) is mostly applied in turning, milling, and grinding. Low-frequency vibration assistance (less than 1000 Hz) is applied in drilling and unconventional machining methods including EDM and ECM [1–3]. Compared to high-frequency

vibration-assisted machining (HVAM), low-frequency vibration-assisted machining (LVAM) has the advantage of improving process performance with less system modifications and cost [8, 9]. In LVAM, higher depth of cut can be achieved compared to HVAM because the amplitudes of assisted vibration are usually higher, which induce high dynamic load. Hence, higher material removal rate can be achieved with the application of LVAM. In addition, the contact between the tool and the workpiece sustains for a longer period, as well as longer time of separation between the tool and the workpiece compared to HVAM. This enables efficient lubrication and cooling effect rather than only cooling effect in HVAM.

Limited research was reported with respect to LVAM. Low-frequency vibration was first applied by R.C. Skelton with the frequency of 0–125 Hz in turning [4, 8]. Lower cutting forces, cutting temperature, tool wear, and improved surface finish were reported, which was attributed to periodic separation of tool and workpiece. Kim et al. [9] performed low-frequency turning at 300, 400, and 500 Hz in machining of aluminum and STAVAX. Uniform textured surface was generated due to the vibration. Low-frequency vibration was first applied in drilling process by Adachi and Arai [10]. Extended tool life, reduced burr formation, and improved quality of hole in vibration-assisted drilling was reported. The effect of both high-frequency and low-frequency assistance in milling was studied by Chern et al. [11] with the frequency range of 100 Hz, 1 kHz, and 10 kHz. Higher dimensional accuracy and lower surface roughness was observed with low-frequency assistance of 1 kHz. Low-frequency assisted milling produces miniature discontinuous chips, which improves the accuracy of machined component. Most of the literature for low-frequency vibration assistance was observed in drilling process, which aimed at machining high-strength materials, composites, and polymers [2, 10]. This indicates that LVAM is capable of significantly improving the machining performance.

Based on the literature, the effect of low-frequency vibration on the effective cutting stresses, residual stresses, and influence of workpiece material properties on low-frequency vibration-assisted turning (LVAT) was not reported. This paper presents the study on low-frequency vibration-assisted turning for three aerospace materials, including Ti6Al4V, AISI 4340 steel, and Al 2024-T351. Electromagnetic vibrators are used to produce vibrations with amplitude less than 0.3 mm and vibration frequency lower than 1000 Hz. These electromagnetic vibrators are easy to be implemented in the turning machine. Effective stresses, cutting temperature, instantaneous cutting forces, and residual stresses are simulated by finite element modeling with experimental validation. Tool wear and machined surface quality are characterized experimentally.

2 Finite element modeling and simulation

3D orthogonal turning model is developed in ABAQUS software. Dynamic explicit temp-displacement solver is used to analyze both mechanical and thermal aspects of turning process [12]. The cutting tool is tungsten carbide (WC) and is assumed to be rigid in order to reduce the computational time in the simulation. Coupled temperature-displacement element type of Hex-dominated shape is used with an allowance of maximum element growth for higher accuracy, shown in Fig. 1. This element model facilitates the calculation of both mechanical and thermal changes. A convergence study is performed, and it is found that the variation in outputs (cutting force, effective stress, and temperature) is less than 5% when the element number is beyond 68,892. This mesh density reduces the size of each element to be less than 1 μm^3, which ensures adequate simulation accuracy.

Cutting velocity is applied on the workpiece, and the tool is provided with vibration assistance along the direction of cutting velocity. The primary cutting edge of the tool in experiments is perpendicular to the work surface, and the secondary cutting edge has an angle of 5° with the surface. This satisfies the conditions of orthogonal machining, and the comparison is conducted [13]. The frictional properties at the interface are defined by modified Coulomb's friction law considering the sticking and slipping phenomenon of chip on the rake face. The sticking region is dependent on shear stress of the material with plastic flow. If the material is under the stress beyond the threshold shear stress value, it starts flowing on the rake face. This property is used in the finite element analysis (FEA) simulation to approximate the actual friction conditions in machining [14].

The properties of workpiece, cutting tool, and cutting conditions in the finite element (FE) simulations are specified in Table 1. Low cutting speeds and high feeds are considered to evaluate the tool wear, surface finish, and built-up edge (BUE) formation, as the effect of vibration is prominent at low cutting speeds [7]. The cutting parameters are selected such that the vibration velocity exceeds the cutting velocity, which enables intermittent cutting. Due to the difficulty of imposing boundary condition considering the coolant in the FE model, dry machining is performed to determine the effectiveness of LVAT process compared with conventional turning (CT). The simulation parameters used in the model are presented in Table 2. The total time of machining in this simulation is 0.01 s,

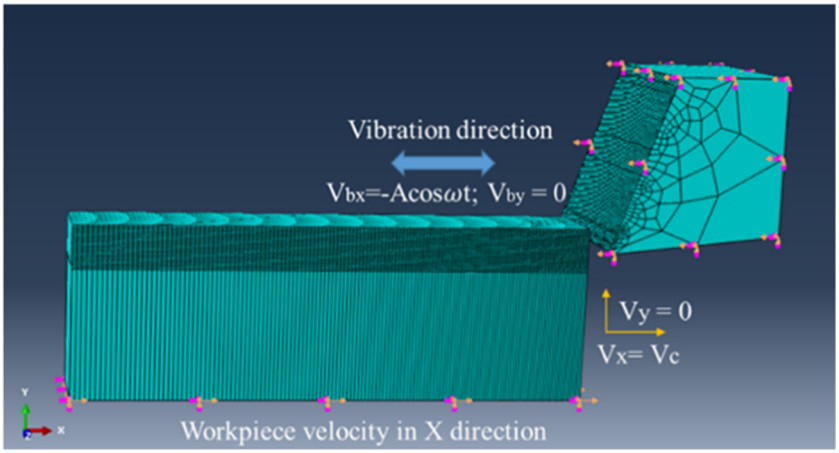

Fig. 1 3D finite element model in ABAQUS showing element mesh and boundary conditions

which generates 5 cycles of vibration as frequency of vibration assistance is 500 Hz and the amplitude is 0.2 mm.

2.1 Material property model for workpiece

Material constitutive model of the workpiece plays a key role in the chip formation and cutting force generation in the simulation process. The Johnson-Cook (JC) model is used since it is able to model the flow stress at high strain rates [15]. In this model, the effect of strain hardening of material at high strain rate and the thermal softening effect are considered for machining purpose. The JC equation is an empirical model expressed as Eq. (1) [16].

$$\sigma_{\mathrm{eq}} = [A + B(\varepsilon)^n]\left[1 + C.ln\left(\frac{\varepsilon^o}{\varepsilon_0^o}\right)\right]\left[1 - T^{*m}\right] T^* = \frac{T - T_{\mathrm{room}}}{T_{\mathrm{melt}} - T_{\mathrm{room}}} \quad (1)$$

where σ_{eq} is the equivalent stress, ε is equivalent plastic strain, $\dot{\varepsilon}/\dot{\varepsilon}_{\dot{A}}$ is the reference strain rate, T_{melt} is the melting temperature, and T_{room} is the room temperature. A, B, C, n, and m are material constants, where A is the initial yield stress, B is the hardening modulus, C is the strain rate-dependent coefficient, n is the work-hardening exponent, and m is the thermal softening coefficient. This empirical model produces acceptable solutions to applications such as penetration, impact, and explosive

Table 1 Properties of workpiece, tool, and cutting conditions

Materials and dimension in simulation	Workpiece: Ti6Al4V; AISI 4340 steel; Al 2024-T351 (3 × 0.2 × 1 mm^3)
	Cutting tool: tungsten carbide (0.8 × 0.8 × 0.8 mm^3)
Machining conditions and dimensions	Simulation
	Speed 30 m/min
	Depth of cut 0.1 mm
	Width of cut 0.2 mm
	Coefficient of friction (μ) 0.4
	Tool angles: rake angle 10° and clearance angle 5°
	Edge radius: of 40 μm (cutting edge not perfectly sharp)
	Dry cutting
	Experimentation
	Speed 30 m/min (diameter of workpiece 35 mm)
	Depth of cut 0.2 mm
	Feed: 1.03 mm/rev
	Tool geometry: side cutting edge angle 0°, end cutting edge angle 5°. Nose angle 85°

Table 2 Simulation parameters used in the FE simulation

Solution procedure	Dynamic-temp-disp-explicit
Element type	Coupled temperature-displacement: explicit type
	Geometric order: linear; element: C3D8RT
Meshing	ALE adaptive mesh: frequency 100; remeshing sweeps per increment: 1
Element distortion control	Length ratio 0.1
Interactions	General contact: tool-master surface, workpiece-slave surface
Interface friction	Tangential behavior: penalty contact: coefficient of friction 0.4
	Modified Coulomb friction law with threshold shear stress 290 MPa (which defines sticking region) [14]
Element deletion	Yes
Heat generation	Inelastic heat fraction 0.9; gap heat generation $\eta = 1, f = 0.9$
Boundary condition	Tool vibrating along cutting direction-periodic amplitude and workpiece has cutting velocity 30 m/min

Table 3 Material modeling data for Ti6Al4V used in simulation

Density					4420 kg/m^3	
Conductivity					7.264 W/m °C	
Young's modulus					114 GPa	
Specific heat					526 J/kg °C	
JC model parameters [7]						
A (MPa)	*B* (MPa)	*C*	*n*	*m*	Melting temperature (°C)	Reference strain rate (s^{-1})
724.7	683.1	0.035	0.47	1	1650	2000

acceleration of metals. The parameters used in modeling the workpiece are listed in Table 3.

Johnson-Cook failure model is employed to simulate the material deformation and chip formation. This is based on the equivalent plastic strain at element integration points. According to JC model, the damage parameter D is defined in Eq. (2), where $\Delta\varepsilon^{pl}$ is the incremental equivalent plastic strain, which is updated at every incremental simulation time; ε_f is the equivalent strain at material failure. Failure of the material occurs when D is greater than or equal to one. $\Delta\varepsilon^{pl}$ depends on equivalent plastic strain, the ratio of hydrostatic stress or mean stress to Von-Mises equivalent stress is p/q, $d1$~$d5$ are the damage constants, and T^* is the same as that mentioned in Eq. (1). The damage parameters used in this simulation are listed in Table 4 [17].

$$\varepsilon_f = \left[d_1 + d_2 \exp\left(d_3 \frac{p}{q}\right)\right]\left[1 + d_4 1n\left(\frac{\varepsilon^p}{\varepsilon}\right)\right]\left[1 + d_5 T^*\right] \quad (2)$$

$$D = \sum\left[\frac{\Delta\varepsilon^{pl}}{\varepsilon_f}\right] \quad (3)$$

2.2 Simulation results

The simulations are performed as per the machining conditions specified in Table 1 for CT and LVAT. It is assumed that the results in conventional turning are constant because the variation in outputs are insignificant compared to that in LVAT. All the output parameters (stress, force, temperature, and residual stresses) are estimated in one complete cycle for LVAT.

Table 4 Damage constants for Ti6Al4V used in simulation [16]

*d*1	*d*2	*d*3	*d*4	*d*5
−0.09	0.28	0.48	0.014	3.18

2.2.1 Simulation for conventional turning of Ti6Al4V

The cutting force, temperature, and stress obtained in CT for Ti6Al4V are shown in Fig. 2. The average stress developed in CT is 1300 MPa (Fig. 2a). The maximum cutting temperature is approximately 331 °C (Fig. 2b) with the average temperature of 322 °C. The average tangential cutting force is 155 N (Fig. 2c). Residual stress is dominant in circumferential direction compared to axial and radial directions [18–22]. Residual stress of the machined surface behind the cutting zone is analyzed after the simulation reaches steady state with complete retraction of tool considering the springback effect. The values are recorded at various locations as shown in Fig. 2d, and the average value is obtained. The variation of the residual stress along the depth is evaluated from the simulation. The average values at various depths below the machined surface at an interval of 15 μm are calculated. It is found that the residual stresses are mostly tensile with a maximum of 359 ± 23 MPa at the surface and gradually diminish after 100 μm depth from the surface. The residual stresses at a few locations at 80 μm depth are compressive; however, the magnitude is less compared to tensile residual stress, and its effect is less compared with other locations at the machined surface.

2.2.2 Simulation results for LVAT of Ti6Al4V

The simulation results for LVAT of Ti6Al4V are presented in Figs. 3 and 4. The process is divided into four stages: stage 1, the tool approaches to the workpiece, defined as initial penetration; stage 2, complete penetration into the workpiece; stage 3, partial retraction of tool from workpiece; and stage 4, complete retraction of tool from workpiece. In the FE simulations, the average stress developed at stage 1 is 768 MPa and the average stress developed at stage 2 is 1289 MPa, which can be considered as the peak stress in LVAT due to added impact energy. In some time instances, stress at stage 2 in LVAT is higher than that in CT (about 5–8% higher than CT). However, the average stresses are lower compared to those

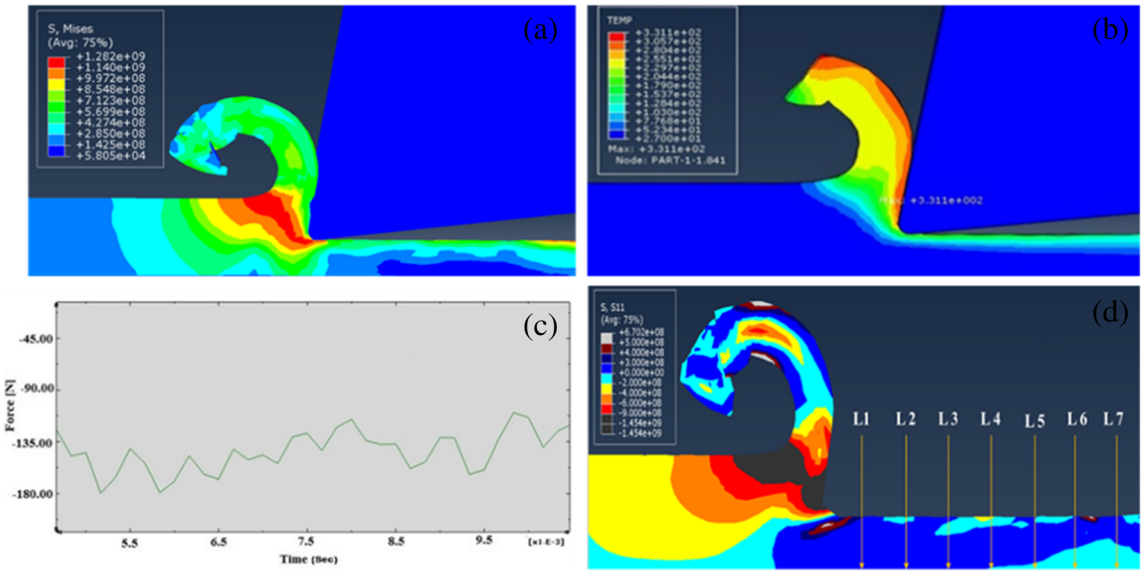

Fig. 2 **a** Effective stresses (MPa). **b** Maximum cutting temperature (°C). **c** Cutting force (N). **d** Residual stress (MPa) observed in CT of Ti6Al4V

in CT as the contact is not continuous. It is observed that as the amplitude of the vibration increases, the amount of stress developed in the workpiece also increases. The stress in stage 3 is 608 MPa and stage 4 is 532 MPa, which indicates stress release of the workpiece in the material deformation region.

The temperature generated in LVAT is 305 °C, which is lower than that in CT. This is due to the availability of time for heat dissipation from the machining zone when the tool is out of contact with the workpiece. The temperature distributed in chip and workpiece for LVAT is presented in Fig. 4a. The temperature decreases at material interface and is shown in Fig. 4b at the instance of retraction of tool in LVAT. The minimum temperature recorded in LVAT is 275 °C. The average force developed per cycle in LVAT is 120 N, and the maximum force is 155 N which is approximately equal to that in CT; however, the force drops to zero at stage 4 due to intermittent tool-workpiece contact. The force generated in a single tool-workpiece contact cycle in LVAT is shown in Fig. 4c.

3 Experimental validation of the FE model

Turning process of Ti6Al4V is performed on precision lathe Magnum-2000. The workpiece material and tool

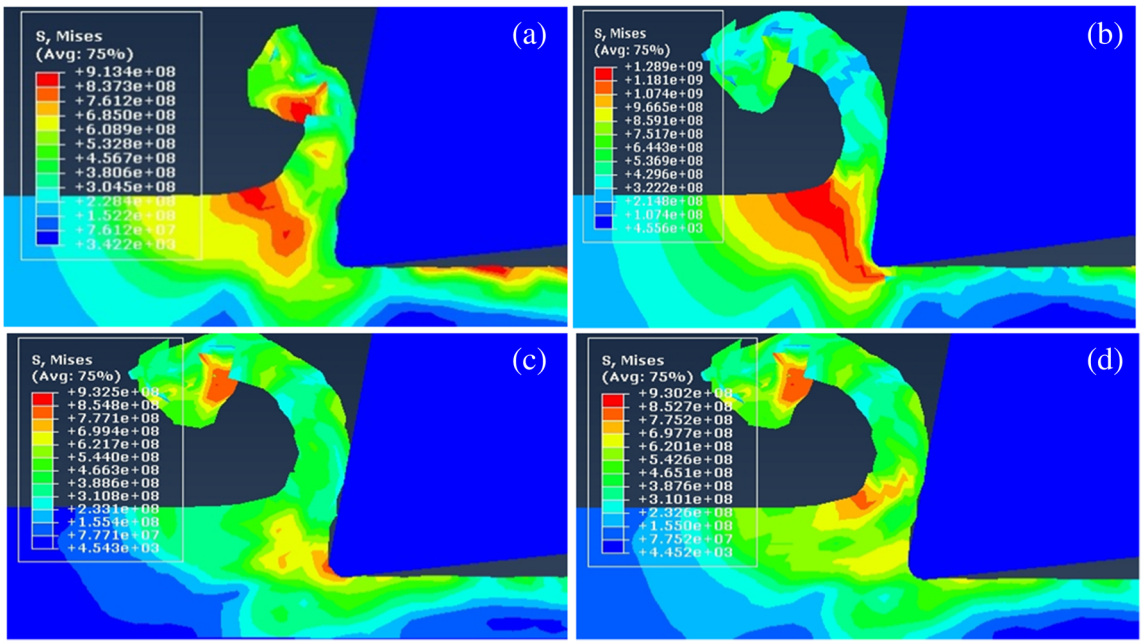

Fig. 3 Effective stress (MPa) in LVAT of TI6AL4V. **a** Stage 1. **b** Stage 2. **c** Stage 3. **d** Stage 4

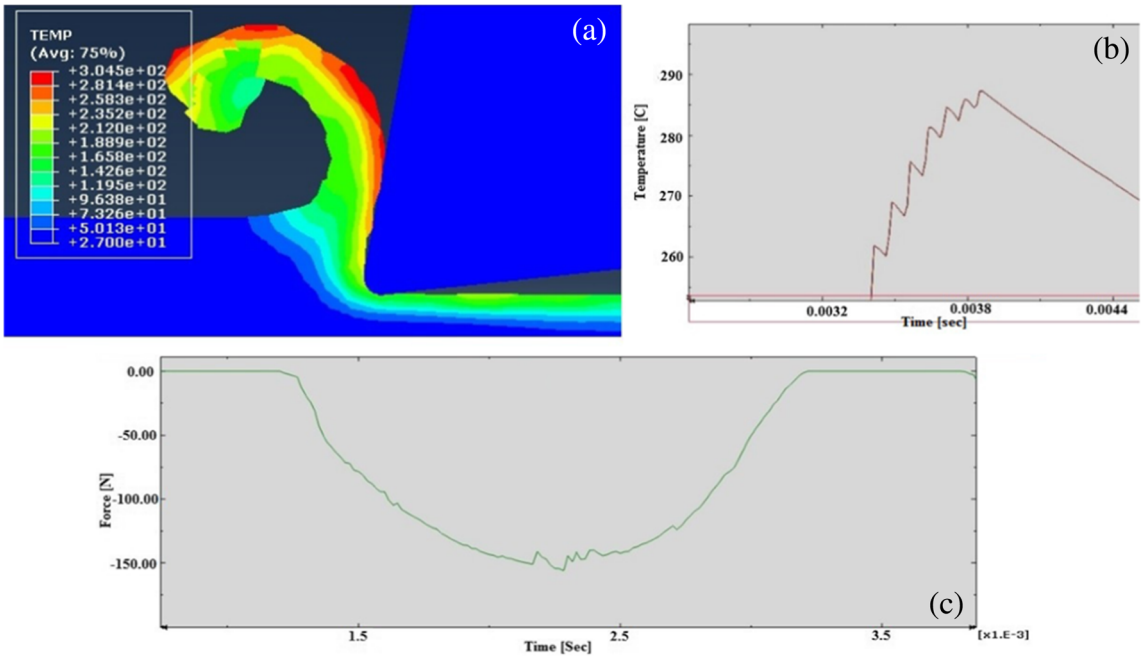

Fig. 4 **a** Average temperature (°C). **b** Decrease in temperature (°C). **c** Cutting force (N), in LVAT for 1 cycle

specifications are mentioned in Table 1. Vibration is generated through an electromagnetic drive, known as eccentric rotating mass vibration motor (ERM) which generates vibrations from the effective eccentric mass attached to the shaft. It can be driven by a DC voltage source at the ERM's rated voltage. The frequency of the vibration is determined by the rotating speed of the motor. Vibration generated by ERM is transferred to tool through direct contact. The modes of vibration and natural frequencies are identified as shown in Fig. 5. The natural frequency in the first mode is 2180 Hz and in the second mode is 1980 Hz, which result in resonant amplitude of 0.75 mm. However, the operating frequency is far below the natural frequency to preserve the stability. It should be mentioned that the direction of the vibration assistance is along the tangential direction, so the vibration assistance does not influence the dynamic chip thickness or the regenerative chatter. The frequency induced is 500 ± 50 Hz and the amplitude of vibration is 200 ± 15 μm, which ensures the basic principle of vibration-assisted machining that vibration velocity exceeds the cutting velocity to result in intermittent cutting.

Cutting forces are measured using a six-component Kistler dynamometer (type 9257B) with data acquisition system (type 5070A) calibrated to a force range of 0 to 500 N. The cutting temperature is measured by Fluke Ti 200 (60 Hz frame rate) thermal imager. The tool wear is measured through Mitutoyo TM-510 tool maker's microscope, and the surface roughness is assessed by Marsurf M400. The residual stresses are analyzed using the Bruker AXS D8 Discover X-ray diffraction machine with Cu-Ka source, and the characterization peak is represented in Fig. 6. There is a slight shift in the peak for machined and unmachined surface. The diffraction images at the

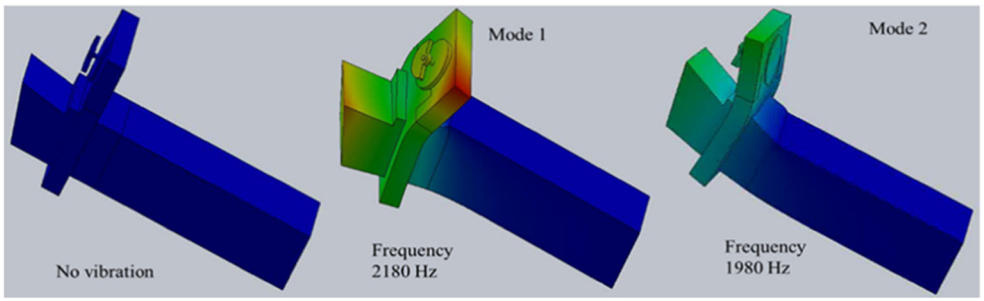

Fig. 5 Modes of vibration and natural frequency of tool setup

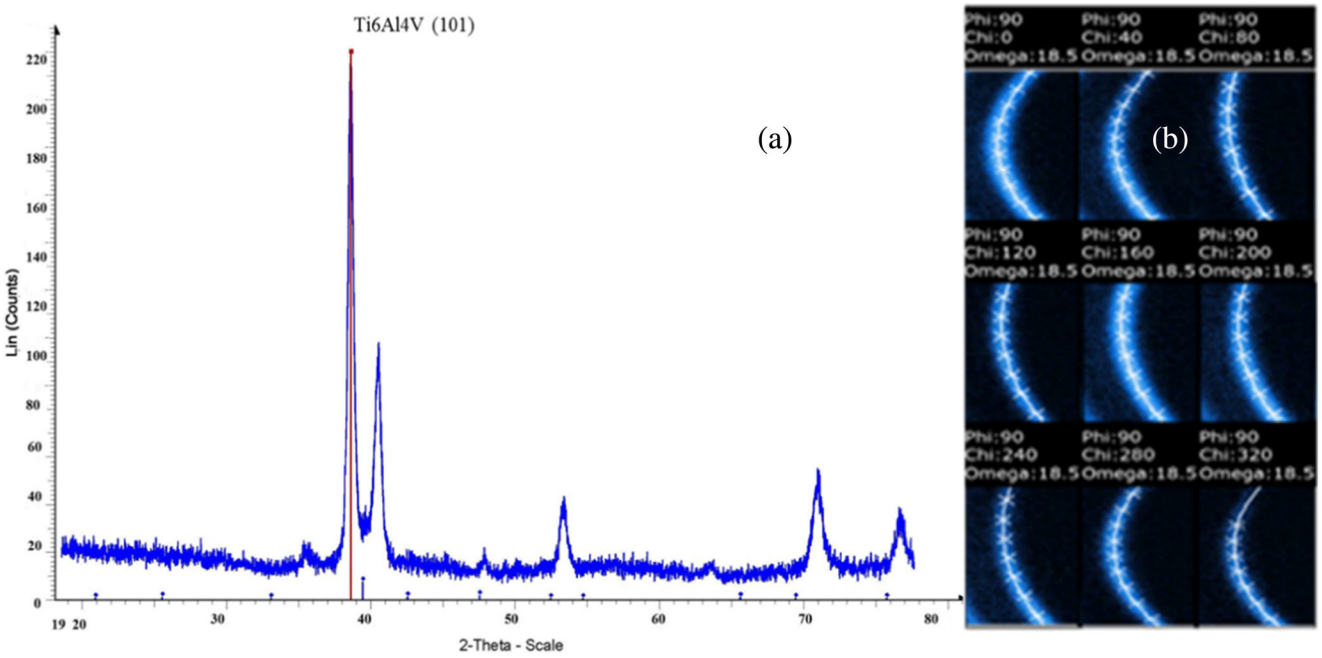

Fig. 6 The X-ray diffraction of Ti6Al4V. **a** Characteristic peak. **b** Stress analysis using Diffrac Leptos software

characteristic peak for various chi angles are analyzed using Diffrac Leptos 6.0 software to predict the residual stress. Leptos software can predict the residual stress for 1D and 2D detector data [23]. 1D data uses classical $sin^2\psi$ method for the prediction of principal and shear residual stresses. 2D data uses XRD^2 [24] method to predict accurate stress distribution compared to 1D classical analysis [25, 26]. Standard 2D data is collected using Chi method of obtaining the data [24]; the Pearson VII method of peak evaluation is used to predict the principal residual stresses.

Cutting forces, temperature, and residual stresses are evaluated in the case of CT and LVAT to validate the FE model. The average cutting force in CT is 140 N (Fig. 7a), and the average cutting force generated in LVAT is 105 N with maximum and minimum forces of approximately 185 and 19 N, respectively (Fig. 7b). The average cutting forces are accessed using the DynoWare (type 2825) module from Kistler. The maximum temperature in CT is reported through the thermal imager as 322 °C (Fig. 8a) and in LVAT as 298 °C (Fig. 8b) which is lower compared to that in CT. The average temperature is also less compared to that in CT. The residual stresses are evaluated for CT to validate the simulation model. The average surface residual stress is tensile and is measured to be 328 ± 55 MPa. It is observed that the simulation and experimental results

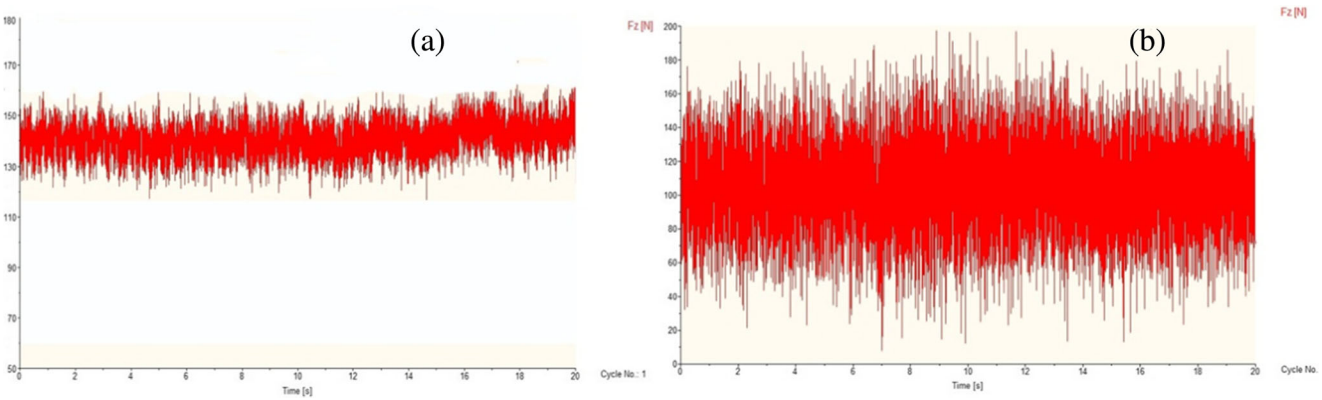

Fig. 7 Cutting forces (N) in **a** CT and in **b** LVAT of Ti6Al4V

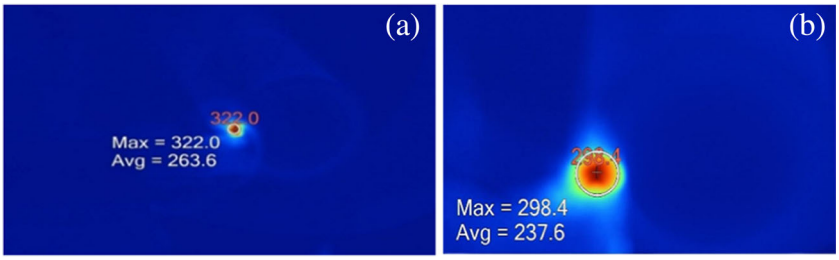

Fig. 8 Temperature (°C) generated in **a** CT and **b** LVAT of Ti6Al4V

are in agreement. In the case of CT, the variation in forces is 7%, and in temperature, it is approximately 3.6%. In LVAT, the variation of forces is 11% and the temperature variation is 2.29%. Based on the comparison, the FE model is validated with approximately 10% difference between the simulations and the experimental results (Table 5).

The 3D simulation model is used to analyze the effect of LVAT on the residual stresses. The residual stresses are evaluated in all three directions for LVAT to identify the effect of vibration assistance. Figure 9 shows the circumferential residual stress (CRS) generated in each stage of LVAT (s11) [20]. In stage 1 (s1), the average CRS is 254 MPa and is predominantly tensile. In stage 2 (s2), the CRS are completely tensile and the average CRS is around 336 MPa. In stage 3 (s3), the CRS is more compressive; about 70% of machined surface is compressive. The average CRS at this stage is −172 MPa. In stage 4 (s4), the CRS are almost similar to those in stage 3, with the average value of −182 MPa. This is due to lower thermal loads, higher mechanical loads, and greater variation and reduction in effective stresses compared to those in CT [18, 19]. The variation in CRS with the depth of machined surface is shown in Fig. 10. In stages 3 and 4, there is about 45% reduction in tensile residual stress, and the maximum compressive residual stress is observed at stage 4.

The variation of axial residual stress and radial residual stress in LVAT is minimal compared with that of CRS [19, 21]. This is because the maximum influence of vibrations pertains only in cutting directions and is negligible in other directions. The variation of axial and radial residual stresses is shown in Fig. 11. It is clearly observed that there is no variation of residual stress during the penetration or retraction. The complete results in LVAT and CT of Ti6Al4V in each stage are compared with those in CT in Fig. 12. The results include effective stresses, cutting forces, cutting temperature, and residual stress in each of the process. From the observed results, it can be inferred that the performance of LVAT is better compared to that of CT for Ti6Al4V, showing the reductions of cutting force, effective stresses, and temperature by 32, 41, and 23% respectively.

In order to confirm the improvements of LVAT over CT, other materials including AISI 4340 and Al 2024 are also assessed by FE simulations and experiments. The materials are selected in such a way that their machinability is less with respect to conventional turning with wide variation in hardness. The variation of the process outcomes in LVAT are presented by each stage of its vibration cycle. To assess the performance of LVAT, tool wear and surface roughness are also evaluated experimentally and are compared to CT.

4 Results and analysis for AISI 4340 and Al 2024

4.1 Machining of AISI 4340 steel (oil hardened)

AISI 4340 is nickel-chromium-molybdenum alloy steel with the hardness of 51–56 HRC. It is known for its toughness and its ability to retain strengths even at high temperature. It is widely

Table 5 Comparison of force and temperature in each process

Parameter	CT		LVAT	
	Simulation	Experimentation	Simulation	Experimentation
Force (N)	155	145	120	114
Temperature (°C)	334	322	305	298
Residual stress (MPa)	356	328	–	–

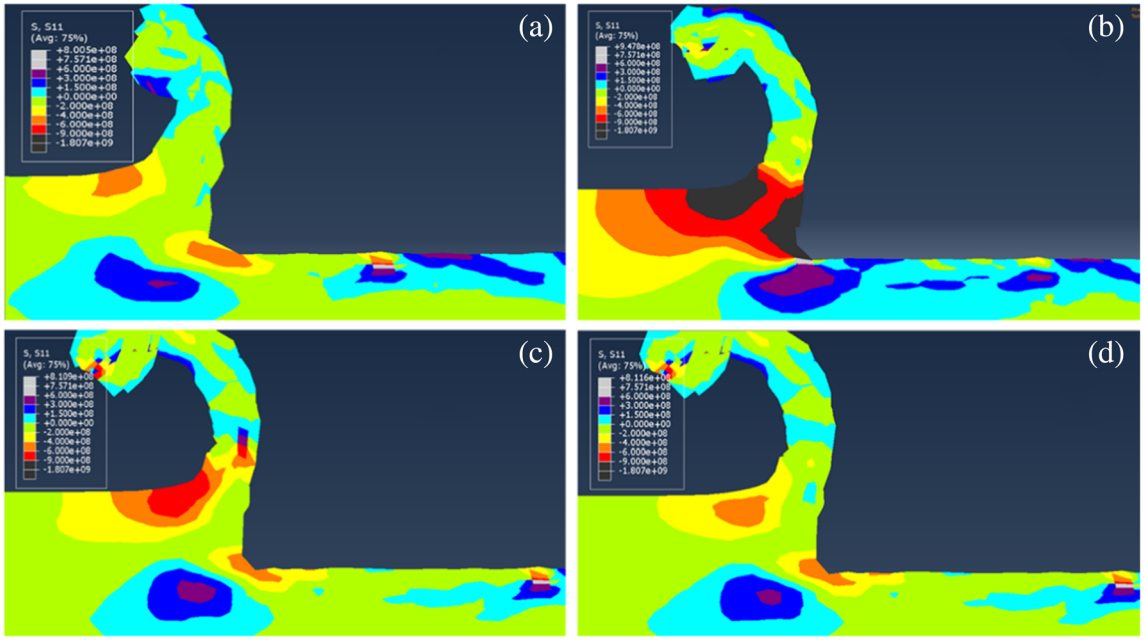

Fig. 9 Variation of CRS (MPa) along **a** stage 1, **b** stage 2, **c** stage 3, and **d** stage 4 in LVAT of Ti6Al4V

used in critical structural components in commercial and military aircrafts such as landing gear, impeller, and frame. Machining of this material involves challenging tasks including low tool life, low geometric accuracy, and low machining efficiency. In this study, FE simulations of conventional and vibration-assisted machining of AISI 4340 steel are conducted, with the material properties and JC material model parameters [27–30] presented in Table 6. The frictional properties mostly depend on material interface rather than machining conditions. The friction property at interfaces are provided by modified Coulomb friction law considering shear factor [14] which defines the sticking region during chip formation [30].

The FE simulations show that the stresses developed in the deformation zone are moderately high, with average value of 2028 MPa in CT. In LVAT process, the stress reaches a maximum of 2043 MPa in penetration and drops to minimum value of 938 MPa at retraction which is about 54% reduction compared to that in CT. Machining temperature developed in CT is 538 °C, whereas in the case of LVAT, the temperature reduces to a minimum value of 442 °C at retraction, which is about 18% reduction. The cutting force in CT is 311 N, while in LVAT, the maximum cutting force is 324 N and the average force is 209 N, which indicates 32% reduction in cutting forces. The residual stress developed in machining of AISI 4340 steel in CT is tensile, and the average tensile CRS is 433 MPa. In LVAT process, a maximum compressive residual stress is found at stage 4 with the value of −273 MPa. The values of stress, temperature, force, and residual stress developed in LVAT of AISI 4340 are represented in Fig. 13.

4.2 Machining of aluminum 2024-T351

Al-2024-T351 is aluminum-based alloy known for its high strength to weight ratio and good fatigue resistance. It is

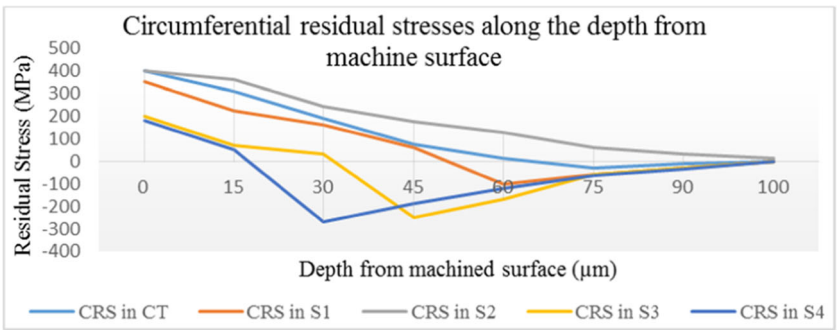

Fig. 10 Variation of CRS (MPa) with respect to the depth (μm) of Ti6Al4V in LVAT and CT

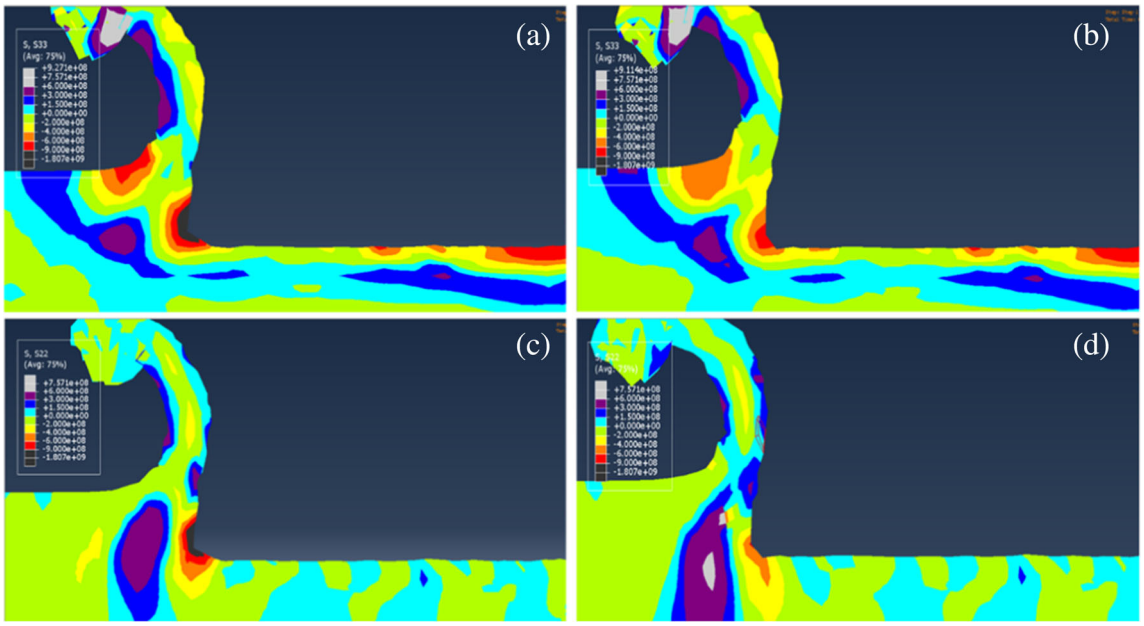

Fig. 11 Variation of axial residual stress (MPa), **a** penetration and **b** retraction; variation of radial residual stress (MPa), **c** penetration and **d** retraction in LVAT of Ti6Al4V

widely used in aircraft fittings, missile parts, gears and shafts, couplings, fastening devices, veterinary and orthopedic equipments, and structures. Machining of this material involves continuous chips and formation of BUE at low speeds, which further lead to increased cutting forces and reduced surface finish. The material model properties and JC model [31, 32] are presented in Table 7. The friction coefficient is higher than steel and Ti alloy [14, 33] which is due to the adhesion of aluminum alloys.

The FE simulations show that the effective cutting stress is approximately 540 MPa in CT process. In LVAT, the maximum stress is 588 MPa and the minimum stress is 298 MPa, which indicates that there is about 44.8% reduction in stresses with the application of vibration assistance. The minimum temperature in LVAT is 100 °C and for CT is 143 °C. Hence, the average drop in temperature of LVAT is 30%. The maximum cutting forces in CT is 95 N. In LVAT, the maximum force is around 105 N and the average value is 60 N, which corresponds to 39% reduction in cutting force. The CRS is compressive in the case of LVAT and is tensile in CT. In CT, the maximum tensile residual stress is 130 MPa. The maximum compressive residual stresses are −86 MPa and the tensile CRS is 128 MPa in the case of LVAT. The simulation results according to different stages in the cycle of LVAT are compared with those in CT in Fig. 14.

5 Characterization of tool wear and surface roughness

5.1 Tool wear analysis

Tool wear and surface finish are critical factors to assess the machining performance. In this study, experimental investigations are conducted to determine the effects of vibration assistance on these two factors. Tool wear is

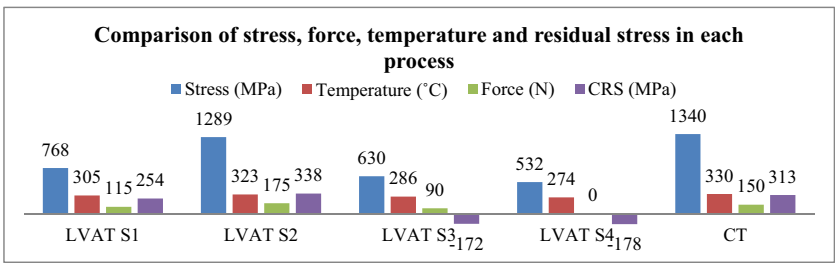

Fig. 12 Comparison of outputs of LVAT and CT in machining Ti6Al4V

Table 6 Material properties of AISI 4340 used in the simulation

Density					7850 kg/m^3	
Conductivity					44.5 W/m °C	
Young's modulus					196 GPa	
Specific heat					475 J/kg-°C	
Poisons ratio					0.3	
Coefficient of friction and shear stress					0.55; 750 MPa [30]	
JC modeling parameters						
Material modeling parameters [27]						
A (MPa)	*B* (MPa)	*C*	*n*	*m*	Melting temperature (°C)	Strain rate
1504	569	0.003	0.22	0.9	1426	2000
Damage parameters [28, 29]						
*D*1	*D*2	*D*3	*D*4		*D*5	
0.05	3.44	−2.12	0.002		0.61	

analyzed for a length of cut of 75 mm in each cutting pass. Four cutting passes are conducted to analyze the tool wear, formation of BUE is observed for both AISI 4340 steel and Al 2014-T351, shown in Fig. 15. It is shown that the

Table 7 Material properties of aluminum 2024-T351 used in the simulation

Density					2700 kg/m^3	
Conductivity					121 W/m °C	
Young's modulus					73 GPa	
Poison ratio					0.33	
Specific heat					857 C	
Coefficient of friction and shear stress					0.6; 200 MPa [14, 33]	
JC modeling parameters						
Material modeling parameters [31]						
A (MPa)	*B* (MPa)	*C*	*n*	*m*	Melting temperature (°C)	Strain rate
352	440.8	0.0083	0.42	1	526	2000
Damage parameters [31]						
*D*1	*D*2	*D*3	*D*4		*D*5	
0.13	0.13	−1.5	0.011		0.58	

and the tool is monitored after each cutting pass and significant wear is observed in the third pass. The five lengths and heights of flank wear are measured under tool maker's microscope Mitutoyo TM-510, and the average is reported in Table 8. In both CT and LVAT processes, maximum height of flank wear in LVAT is larger than that of CT for AISI 4340. However, length of flank wear in LVAT is almost half of that in CT, which can be attributed to the intermittent contact between the tool and workpiece when vibration assistance is applied.

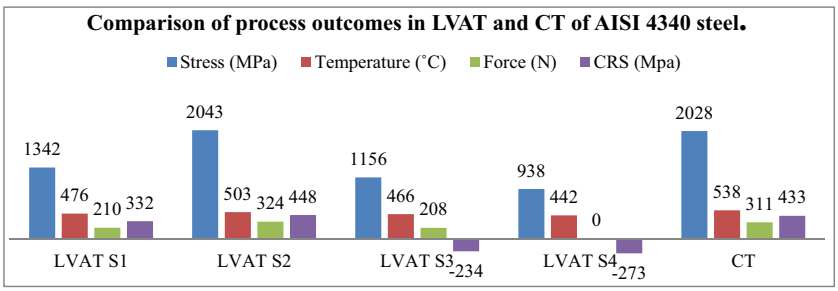

Fig. 13 Variation of outputs between LVAT and CT in machining of AISI 4340

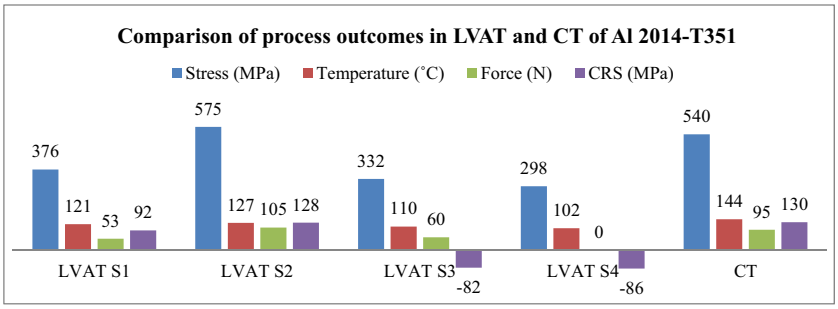

Fig. 14 Variation of output parameters in various stages of LVAT compared to that of CT

Table 8 Comparison of tool wear in CT, LVAT of AISI 4340, Ti6Al4V, and Al 2024-T351

Material	Process	V_B max (mm)	V_B min (mm)	Height of BUE formed (mm)	Length of flank wear (mm)
AISI 4340	CT	0.135	0.027	0.178	1.38
	LVAT	0.134	0.046	0.117	0.649
Ti6Al4V	CT	0.112	0.37	No BUE	1.36
	LVAT	0.138	0.20	No BUE	0.601
Al-2024-T351	CT	0.073	0.043	0.292	1.05
	LVAT	0.065	0.052	0.128	0.604

The tool wear for Ti6Al4V shows that the maximum flank wear in LVAT is slightly higher than that in CT. However, the average height and length of flank wear is minimal compared to those in CT. The length of flank wear is only 0.623 mm, which is almost half of the value compared to that in CT. This indicates that although the maximum V_B occurs in LVAT, the length of wear is minimum. In the case of Al 2014-T351, formation of BUE is observed in CT as well as in LVAT. The maximum height of BUE formed in LVAT is almost half of that occurred in CT. The length of wear is less in the case of LVAT with about 35% decrease. Based on the comparison results, it can be inferred that the tool wear in LVAT is greater for AISI 4340 steel compared to that in CT, however, lower in the case of Ti6Al4V and AMS 4037. Hence, it is concluded the LVAT reaches better tool wear performance at moderate and lower at harder materials.

Table 9 Comparison of surface roughness parameters for AISI 4340, Ti6Al4V, and Al 2024-T351 in CT and LVAT

Material	Process	Ra (μm)	Rz (μm)	Rsk
AISI 4340	CT	1.134	6.139	−0.43
	LVAT	1.213	7.856	−0.10
Ti6Al4V	CT	1.142	5.878	−0.17
	LVAT	0.987	5.219	0.113
Al 2024-T351	CT	1.137	6.438	−0.23
	LVAT	0.970	5.108	0.033

5.2 Analysis of surface roughness

In machining of AISI 4340, the comparison of average roughness parameters is shown in Table 9. It is observed that the surface roughness in LVAT is higher than in CT. From Rz result, it can be inferred that the difference in average heights of peaks and valleys is high in the case of LVAT. Both profiles are skewed upwards and indicate high peaks inferred from Rsk. The surface roughness parameters in the case of Ti6Al4V show that the profile is skewed upward relative to the average line and has high peaks density above the average line. The profile has a positive Rsk, which indicates the profile has lower peaks and has high density in valleys. Positive value of Rsk indicates that the surface has scratches or pore-like structure; this is due to the vibration induced by ERM. The vibration assistance causes plowing action in the material deformation zone, hence results in high density of valleys compared to peaks.

For Al 2024-T351, the average roughness in CT is high compared to that in LVAT. The average heights of peaks and valleys are low in the case of LVAT. The surface of CT has skewed downwards and has high density of peaks. In LVAT, the Rsk is positive and is approximately zero,

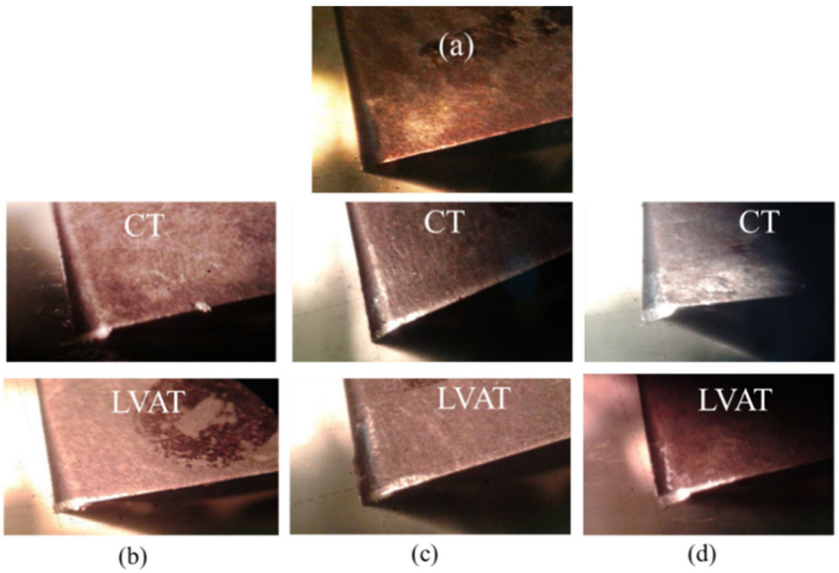

Fig. 15 Tool wear in CT and LVAT for **a** new tool, **b** AISI 4340, **c** Ti6Al4V, and **d** Al 2014-T351

which means the profile is uniformly distributed over the average line with slightly high density of valleys. The surface roughness is maximum in CT and minimum in LVAT for Ti6Al4V and Al 2024-T351. However, the roughness value in machining of AISI 4340 steel is larger in LVAT compared to that in CT.

6 Conclusions

In this paper, FE simulations of conventional and low-frequency vibration-assisted turning are conducted for three aerospace materials: Ti6Al4V, AISI 4340, and Al 2024-T351. Effective stress in the material deformation zone, cutting force, temperature, and residual stress are predicted with experimental validation. BUE, tool wear, and surface roughness are characterized and evaluated experimentally. The following conclusions are drawn based on the results:

1. The FE simulations show that the vibration assistance in LVAT causes the reduction of effective stress, cutting force, and average temperature by 40, 33, and 22%, respectively, in turning of Ti6Al4V. It is due to the stress release when tool retracts from the workpiece periodically. The simulations are experimentally validated. The FE simulations further demonstrate that the vibration assistance is capable of reducing effective stress, cutting force, and temperature approximately by 45, 35, and 25% in turning AISI 4340 and Al 2024-T351.
2. The residual stresses are compressive in stages 3 and 4 of each vibration cycle of LVAT, and the surface residual stresses are predominantly compressive. This is due to lower thermal loads, higher mechanical loads, and reduction in effective stresses. On the other hand, there is no considerable variation in effective stress, and the surface residual stresses are predominantly tensile in CT process. The change in residual stress in axial and radial directions is negligible because the effect of vibration is active only in circumferential direction.
3. LVAT for Ti6Al4V and Al2024-T351 results in lower tool wear rate and surface roughness compared to CT. However, it is the opposite in machining AISI 4340 steel. This may be because the induced vibration is damped out due to high external reaction force when machining high-strength AISI 4340 steel, and the efficiency of vibration assistance reduces. Hence, it can be concluded that LVAT is more effective in improving the tool life for soft and medium hard materials compared to that for high-strength materials. Low excitation energy and the resistance of highly hard materials may damp low-frequency vibrations in LVAT process.
4. LVAT is advantageous in machining the above-mentioned aerospace materials because intermittent cutting action results in the reduction in forces, effective stresses, and temperature. Furthermore, the vibration assistance is beneficial to the chip removal due to the harmonic motion of tool, therefore improving the surface finish and reducing the tool wear.

References

1. Brehl DE, Dow TA (2008) Review of vibration-assisted machining. Precis Eng 32:153–172
2. Kumar MN, Kanmani Subbu S, Vamsi Krishna P, Venugopal A (2014) Vibration assisted conventional and advanced machining: a review. Procedia Eng 97:1577–1586
3. Thoe TB, Aspinwall DK, Wise MLH (1998) Review on ultrasonic machining. Int J Mach tool Manu 38(4):239–255
4. Skelton RC (1969) Effect of ultrasonic vibration on the turning process. Int J Mach Tool D R 9:363–374
5. Babitsky V, Kalashnikov A, Meadows A, Wijesundara AAH (2003) Ultrasonically assisted turning of aviation materials. J Mater Process Technol 132:157–167
6. Ding H, Ibrahim R, Cheng K, Chen S-J (2010) Experimental study on machinability improvement of hardened tool steel using two dimensional vibration-assisted micro-end-milling. Int J Mach Tools Manuf 50(12):1115–1118
7. Patil S, Joshi S, Tewari A, Joshi SS (2014) Modelling and simulation of effect of ultrasonic vibrations on machining of Ti6Al4V. Ultrasonics 54:694–705
8. Skelton RC (1968) Turning with an oscillating tool. Int J Mach Tool D R 8:239–259
9. Kim HS, Kim SI, Lee KI et al (2009) Development of a programmable vibration cutting tool for diamond turning of hardened mold steels. Int J Adv Manuf Technol 40:26–40
10. Adachi K, Yoshikawa A, Sakurai K (2004) A study on burr low frequency vibratory drilling. Mater Forum 28:178–183
11. Chern GL, Chang YC (2006) Using two-dimensional vibration cutting for micro-milling. Int J Mach Tools Manuf 46:659–666
12. .ABAQUS (2014), CAE user guide. Version 6.13
13. Ma J, Duong NH, Lei S (2014) Numerical investigation of the performance of microbump textured cutting tool in dry machining of AISI 1045 steel. J Manuf Process 19:194–204
14. Özel T, Zeren E (2005) A methodology to determine work material flow stress and tool-chip interfacial friction properties by using analysis of machining. J Manuf Sci Eng 128(1):119–129
15. Teng X, Wierzbicki T (2006) Evaluation of six fracture models in high velocity perforation. Eng Fract Mech 73:1653–1678
16. Johnson GR, Cook HW (1985) Fracture characteristics of three metals subjected to various strains, strain rates, temperatures and pressures. Eng Fract Mech 21:31–48
17. Yancheng Z, Outeiro JC, Mabrouki T (2015) On the selection of Johnson-Cook constitutive model parameters for Ti-6Al-4V using three types of numerical models of orthogonal cutting. Procedia CIRP 31:112–117
18. Henriksen EK (1951) Residual stress in machined surfaces. Trans ASME 73:69–76
19. Thiele JD, Melkote SN (2000) Effect of cutting-edge geometry and workpiece hardness on surface residual stresses in finish hard turning of AISI 52100 steel. J Manu Sci Eng 122:642–649
20. Schulze V, Zanger F (2011) Numerical analysis of the influence of Johnson-cook material parameters on the surface integrity of Ti-6Al-4V. Procedia Eng 19:306–311
21. Dahlman P, Gunnberg F, Jacobson M (2004) The influence of rake angle, cutting feed and cutting depth on residual stresses in hard turning. J Mater Process Technol 147:181–184
22. Ahmed N, Mitrofanov AV, Babitsky VI, Silberschmidt VV (2006) Analysis of material response to ultrasonic vibration loading in turning Inconel 718. Mater Sci Eng 424:318–325
23. .Bruker AXS (2009) LEPTO DIFFRAC plus LEPTOS User Manual 2009
24. He BB (2003) Introduction to two-dimensional X-ray diffraction. Powder Diffract 18(2):71–85
25. He BB, Preckwinkel U, Smith KL (1998) Advantages of using 2D detectors for residual stress measurements, advances in X-ray analysis, 47th Annual Denver X-ray Conference, Colorado Springs, USA
26. He BB, Preckwinkel U, Smith KL (1999) Fundamentals of two-dimensional X-ray diffraction (XRD2). Adv X-ray Anal 43:273–280
27. Özel T, Karpat Y, Srivastava A (2008) Hard turning with variable micro-geometry PcBN tools. CIRP Ann-Manuf Technol 57:73–76
28. .Gray GT, Chen SR, Wright W, Lopez MF (1994) Constitutive equations for annealed metals under compression at high strain rates and high temperatures. New Mex los Alamos Natl Lab 21–28.
29. Banerjee B (2007) The mechanical threshold stress model for various tempers of AISI 4340 steel. Int J Solids Struct 44:834–859
30. Arrazola PJ, Ozel T (2010) Investigations on the effects of friction modeling in finite element simulation of machining. Int J of Mech Sci 52:31–42
31. Asad M, Girardin F, Mabrouki T, Rigal JF (2008) Dry cutting study of an aluminium alloy (A2024-T351): a numerical and experimental approach. Int J Mater Form 1:499–502
32. Lesuer DR (2000) Experimental investigations of material models for TI-6Al-4V titanium and 2024-T3 aluminum. Off Aviation Res Washington:1–41
33. Daoud M, Chatelain JF, Bouzid A (2015) On the effect of Johnson Cook material constants to simulate Al2024-T3 machining using finite element modeling. Int J Adv Manuf Technol 81:1987–1997